Permeability Characterization of Sheared Carbon Fiber Textile Preform

Robert S. Pierce,[1,2] **Brian G. Falzon,**[2] **Mark C. Thompson**[1]

[1]*Department of Mechanical and Aerospace Engineering, Monash University, Melbourne, Victoria, 3800, Australia*

[2]*School of Mechanical and Aerospace Engineering, Queen's University, Belfast, BT9 5AH, United Kingdom*

Fabric deformation alters its local permeability characteristics which, in turn, influences the resin infusion process. This work investigates the radial permeability test method of sheared carbon fiber textile reinforcement materials for the purposes of infusion modeling. A novel experimental approach is described, which utilizes a customized Matlab video processing code to track fluid flow and calculate permeability using data from the complete flow field. Results show principal permeability values, K_1 and K_2, to increase and decrease, respectively, from a near isotropic state as the fabric shear angle increases, yielding a K_1/K_2 ratio of 3.74 at the maximum measured shear angle of 40°. Detailed statistical analysis revealed significant error for cases where fewer than 16 measurement directions were used for the permeability calculation, particularly in highly anisotropic samples. POLYM. COMPOS., 00:000–000, 2016. © 2016 Society of Plastics Engineers

INTRODUCTION

The aerospace industry is focused on the development of efficient, lightweight composite aerostructures at reduced manufacturing costs. Liquid Composite Molding (LCM) techniques offer significant potential in achieving both these goals, where dry reinforcement materials are formed to a desired geometry then infused with resin. Furthermore, the drive toward manufacturing larger integrated structures in the future inevitably leads to more complicated geometries, for which highly-drapable woven carbon-fiber composite reinforcements are most suitable. For components with significant double curvature (such as a hemisphere) fabric yarns can shear by as much as 40°–50°, depending on the material [1]. However, the development of an effective LCM strategy for new parts can be challenging, often requiring costly trial-and-error practices and a highly skilled operator. Numerical process

modeling shows great potential in reducing many of these time-consuming and wasteful practices. For modeling purposes, the LCM process is typically divided into three main stages: (i) the physical draping of material, (ii) the subsequent resin infusion, and (iii) cure kinetics. Draping models predict the deformation of dry textile reinforcement materials as they are formed to complex shapes [1–4]. This deformation is dominated by shearing, where "shear angle" (the angular change of yarn orientations from their original state) is the common metric of measurement. Infusion modeling, on the other hand, aims to simulate the flow of resin through the preformed textile material [5–7]. Hence, a realistic model requires the results from draping to incorporate the effects of material deformation on the infusion [8]. Permeability, as the key parameter governing infusion, is particularly important for simulating the manufacture of complex parts. This article focuses on a semi-automated optical method for the characterization of anisotropic textile permeability with improved statistical confidence, in support of LCM process modeling.

Textile Permeability

Permeability is a measure of how easily a fluid flows through porous material under the influence of a driving pressure gradient. During infusion, Newtonian resins travel at low velocities, therefore the flow behavior is typically described by Darcy's law in *Eq. 1*, where v is the volume-averaged flow velocity vector, K is the permeability tensor for the material, μ is the viscosity of the fluid and ∇P is the pressure gradient:

$$v = -\frac{K}{\mu} \cdot \nabla P \tag{1}$$

Though textile materials exhibit a convenient periodic geometry, textile permeability characterization has several complications. Firstly, these materials typically exhibit deformation-dependent anisotropic flow, with an elliptical-shape [9].

Hence, textile permeability must be defined for at least two in-plane principal directions, commonly termed K_1 and K_2 [10, 11], representing the maximum and minimum, respectively. Secondly, there are two different scales of flow that occur within textile preforms: capillary flow between the fibers inside yarns, governed by surface tension, and the simultaneous viscous flow between yarns [12]. Moreover, the tow geometry and spacing are stochastically variable throughout the textile material, meaning that permeability values should really be considered as a statistical distribution rather than clear deterministic values. This is reflected by experimental studies in literature, where identical tests performed in the same lab yielded results with relative standard deviations of over 30%, and comparative tests from different labs varied by whole orders of magnitude [13], attributed also to different processing conditions. Furthermore, recent work has demonstrated the significance of dry fabric handling on material properties, which may also influence the permeability properties [14]. It is not surprising then that there are no standardized methods for permeability characterization, even though several methods are well established and used in industry. However, it must also be noted that the latest round of international benchmarking efforts have shown a significant improvement in 1D permeability characterization [15], suggesting that standardization may yet be possible.

During draping, the permeability of a textile reinforcement material is also affected by local changes in porosity and fiber orientation, with several authors reporting permeability changes of more than 50% when fabrics are highly sheared [16–19]. In simple parts, this is not likely to be an issue, as the porosity is expected to remain somewhat uniform throughout the textile. However, in a complex part with large changes in local porosity and shear angle, an inferior infusion strategy is more likely to result in dry spots or voids that can lead to part rejection in a quality control assessment. Hence, the determination of fabric permeability is necessary over the full range of shear angles that are likely to result from draping.

Permeability characterization can be performed experimentally, as is most common, or alternatively by simulation [17, 20, 21]. The former is well established and widely practiced, though experimental results are not always repeatable [13]. Predictive permeability modeling, on the other hand, can be efficient and consistent but oversimplifies the flow behavior and still requires experimental work for validation purposes.

Permeability Characterization

Experimental permeability testing is typically performed using either linear flow tests, with a uniform fluid flow through a channel of material in one direction; or radial flow tests where fluid flow begins in the center of material samples and flows outward in all directions. Three-dimensional permeability characterization experiments have also been investigated [22, 23], however for the purposes of infusion through thin preforms, 2D permeability experiments remain the focus of this work. Both approaches have been extensively discussed and analyzed in recent literature [13, 24]. Linear tests often show greater repeatability but are not as good for characterizing unknown anisotropic flow behavior, in which case the principal permeability direction needs to be known prior to testing. Radial permeability tests on the other hand, enable the measurement of the flow front in multiple directions, but are more difficult to control and subsequently their results can be more variable [25].

Measurement techniques in permeability characterization are varied; the displacement of the flow front can be tracked visually, or by using a range of sensors: based on electrical resistance, ultrasonic waves, pressure [26], fiber optics [27], or thermistors [11]. The mass flow rate can be determined by measuring the fluid output through the system, or the pressure field across the sample can be determined from pressure transducers. However, cameras are commonly used to monitor the flow front visually [25, 28]. Ultimately, as there is no standard method, and no clear "best" approach, characterization experiments must be designed for each case according to the purpose of the intended research.

The Permeability and Shear-Angle Relationship

In the literature there are several studies that characterize the relationship between shear angle and permeability in textile reinforcements [17, 19, 29–32], although they are predominantly for glass fiber textiles. Among this work, in each case a constant cavity thickness is maintained as the shear angle is increased, effectively increasing fiber volume fraction at the same time. Work by Hammami et al. [19], using pairs of unidirectional plies that were stitched together at 0° and 90° orientations, reported a near four-fold increase in anisotropy, increasing K_1 values and decreasing K_2 values as the shear angle increased. Slade et al. [30] also observed similar trends, though the composition of the stitched and woven fabrics used was not clear.

In contrast, a study by Endruweit et al. [29] shows experimental and modeling results with a general reduction in both K_1 and K_2 principal permeability values for various fabrics. Similarly, decreasing K_1 and K_2 values for glass fabrics have also been reported in experimental work by Smith et al. [31] and modeling by Loix et al. [17]. In addition, the latter group predicted lower principal permeability values in single-ply tests but greater anisotropy at higher shear angles, when compared with thicker multiple-ply models. Lai et al. [32] experimentally observed increasing anisotropy for both glass and carbon-fiber fabrics, with decreasing principal permeability values, but they actually found higher principal permeability values for tests with fewer plies. This difference is attributed to fabric ply nesting and an increasing fiber volume fraction, with the model by Loix et al. [17] simulating an idealized stacking arrangement. Ultimately, no common

conclusive trends have been observed for the deformation-dependent permeability of textile reinforcement materials.

MATERIALS AND METHODS

Experimental Approach

In order to quantify the link between deformation during draping and subsequent flows during infusion, fabric permeability was characterized for a range of shear angles. As noted earlier, the experimental characterization of permeability has received considerable attention in recent years, although it continues to elude standardization despite promising results for linear permeability tests in recent benchmarking efforts [15]. Hence, the experimental design was carefully planned to ensure that testing was as repeatable, reliable and efficient as possible.

The technique adopted here was to use an unsaturated radial flow experiment to gather flow data in every direction simultaneously, rather than testing multiple directions linearly. This increases the efficiency of the permeability testing process over linear flow experiments, since the anisotropy field can be characterized in a single step. Tests were run under a constant injection pressure, rather than controlling the inlet velocity, as the latter can require very high pressure gradients and in practice is more difficult to enforce. The constant pressure differential was driven by a vacuum through the material, with the fluid reservoir left open to ambient pressure; a standard pressure gauge was used to monitor the vacuum pressure and ensure that it remained constant.

Fabric samples (at various shear angles ranging from 0° to 40°) were sandwiched between a glass plate (6.09 mm thick) and a polycarbonate caul plate (7.31 mm thick) underneath a vacuum bag, as shown in Fig. 1, to create a consistent cavity thickness. Typically, with the use of relatively thin plates there are major concerns that deflection can be a source for error; however, regression analysis serves to identify any such error under these conditions. Batches of at least five samples were tested at each shear angle to evaluate the consistency of the results and account for stochastic effects. White breather cloth was placed around the periphery of the fabric samples to facilitate an even vacuum in all directions within the test cavity, ensuring that it would not affect cavity thickness. As the 300×300 mm samples were only one ply thick, testing was considered solely in two dimensions, neglecting through-thickness flow and gravitational effects. The cavity thickness, h, for all tests was measured as 0.40 mm (± 0.03 mm) across the domain, by subtracting the known plate and bag thicknesses from the total thickness measurements at a variety of locations. For this cavity thickness, the estimated fiber volume fraction of tests ranged from 0.28 to 0.36 (for 0° to 40° shear angles respectively), based on the manufacturer's areal weight specification. Although this fiber volume fraction is low
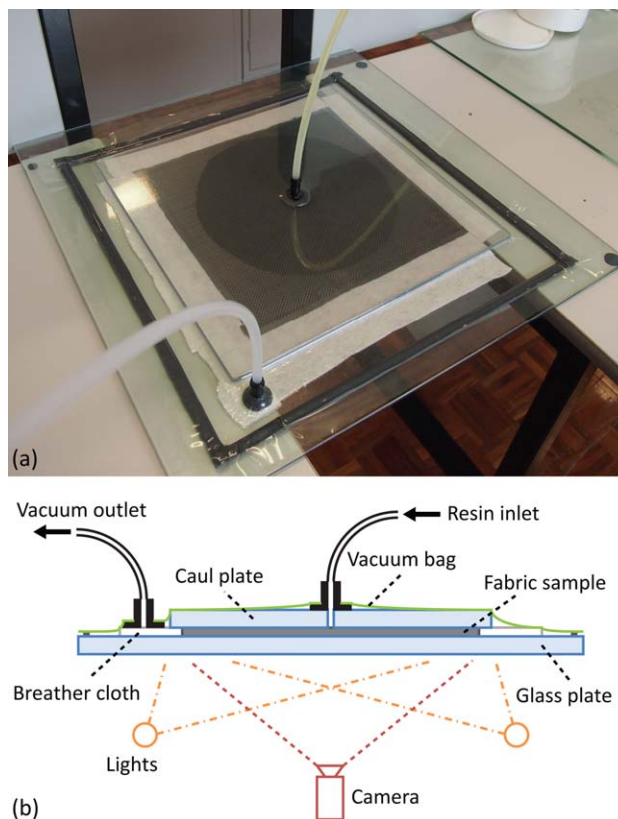

FIG. 1. Experimental set up of (a) an unsheared 0° sample and (b) the full test configuration. [Color figure can be viewed at wileyonlinelibrary.com]

relative to real composite components (more often between 0.4 and 0.5 fiber volume fraction), similar values have been observed in previous permeability studies [31]. Wall effects were likely to be significant in this case, but as they were consistent throughout all tests, the measurements obtained are acceptable for this comparative study, which focuses mainly on the method of analysis. Quantitatively then, the exact permeability values from this study will only be valid for similar, low fiber volume fraction or single ply, cases. If permeability values are desired for more realistic forming applications, a number of stacked preform plies should be tested at a higher fiber volume fraction. A circular inlet port of 6 mm diameter facilitated the flow of the test fluid through the caul plate to the center of each sample.

The radial flow pattern from each test was recorded as a function of time from below the glass plate using a digital video camera, since alternative sensor methods are often more difficult to set up, yield limited data and can negatively affect the flow of the oil through the test cavity [11]. The camera was consistently positioned with the image sensor was parallel to the test plane, at a suitable distance, with a relatively narrow focus lens, such that image distortion was assumed to be negligible (particularly as sample measurements remained near to the center of the images). Video footage was then processed using a novel code to comprehensively characterize the radial

permeability of samples in each test, based on accepted methods, as discussed in the following section.

Materials

Single plies of an aerospace grade, plain weave carbon-fiber fabric (0.193 kg/m^2) with 3K tows were used for these permeability tests. Although testing is more commonly performed with thicker ply stacks, in this case a single-ply test was chosen to eliminate the effect of nesting, and to focus on the deformation-dependent flow properties of the material.

For the infusion fluid, Moro brand "pure" olive oil was used, and was assumed to be Newtonian [33], incompressible, isothermal and chemically inert for the duration of the permeability tests. A cone and plate rotational viscometer was employed to determine the viscosity of the oil for temperatures ranging from 15°C (0.1062 Pa s) to 31°C (0.0561 Pa s).

CALCULATING ANISOTROPIC PERMEABILITY

Theory

The established approach for permeability characterization, based on radial flow through a planar anisotropic material, was introduced by Adams et al. [9]. This describes fluid motion to be governed by the Laplace equation, derived from the continuity equation for incompressible flow combined with Darcy's law. Weitzenböck et al. [10] discuss the implementation of this method, and focus on the definition of anisotropic fabric permeability using two orthogonal principal permeability values, K_1 and K_2 and an orientation angle, φ. Their method determines these values from the transformed isotropic calculation of permeability in three directions (0°, 45°, and 90° relatively). This article briefly discusses the foundations for these methods; however, the full derivations can be found in literature [9, 10].

Initially, isotropy is assumed, thus Darcy's law from *Eq. 1* is rewritten as *Eq. 2*, with regards to the pressure, P, and flow front radius, r. *Equation 2* is combined with the continuity *Eq. 3* in order to determine the radial pressure gradient, $\partial P/\partial r$.

$$v = -\frac{K}{\mu} \cdot \frac{\partial P}{\partial r} \qquad (2)$$

$$\nabla \cdot v = 0 \qquad (3)$$

The radial pressure gradient is then substituted back into *Eq. 2*, accounting for the constant pressure conditions acting across the system. This results in an isotropic flow front velocity vector, v, that is dependent only on flow front radius, r. Then, dividing this superficial velocity vector by the material porosity, ϵ, results in the true radial flow rate in *Eq. 4*, which can be integrated with respect
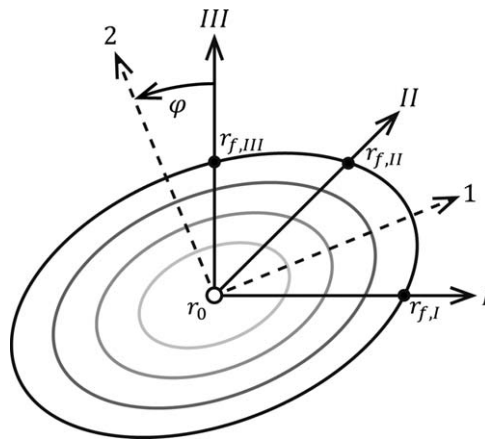

FIG. 2. Principal permeability axes (1 and 2) and measurement directions (*I*, *II*, and *III*) for an advancing radial flow front.

to time (under the conditions $r = r_0$ at $t = 0$, and $r = r_f$ at time t) and rearranged to form *Eq. 5*.

$$\frac{dr}{dt} = \frac{v}{\varepsilon} \qquad (4)$$

$$K = \left[r_f^2\left(2\ln\left(\frac{r_f}{r_0}\right) - 1\right) + r_0^2\right]\frac{1}{t}\frac{\mu\varepsilon}{4\Delta P} = F_i\frac{\mu\varepsilon}{4\Delta P} \qquad (5)$$

This equation defines the isotropic permeability model for experiments with a constant inlet and outlet pressure, for a fixed inlet location. In order to solve this equation, a linear regression is taken for the time history of the bracketed radius term (since the viscosity, porosity and pressure remain constant). The constant gradient, F_i, of this regression line is then used to solve for isotropic permeability, K.

Turning to anisotropic behavior, Weitzenböck et al. [10] derived a set of three equations to define the principal permeability values, K_1 and K_2, and principal permeability direction, φ, for an anisotropic material with 2D radial flow. The full derivation relies on transformations to a quasi-isotropic system and rotation from the measurement axes to the principal axes. This process is similar to the isotropic derivation above, but relies on a symmetric permeability tensor and modified coordinate systems to account for the anisotropic flow behavior and results in *Eq. (6–8)*. These three unknown properties are resolved from measurements in three directions ($I = 0°$, $II = 45°$ and $III = 90°$ relatively), at any orientation. Where $A = (F_I + F_{III})/2$, $D = (F_I - F_{III})/2$, $C = \mu\epsilon/4\Delta P$ and F_I is the regression gradient for the flow front radius in the I direction. Figure 2 shows the relationship between these properties, the principal axes and the measurement directions for an idealized elliptical flow front.

$$K_1 = F_I\frac{(A-D)}{\left(A - \frac{D}{\cos 2\varphi}\right)}C \qquad (6)$$

$$K_2 = F_{III}\frac{(A+D)}{\left(A + \frac{D}{\cos 2\varphi}\right)}C \qquad (7)$$

$$\varphi = \frac{1}{2}\tan^{-1}\left(\frac{A}{D} - \frac{A^2 - D^2}{F_{II}D}\right) \qquad (8)$$

It is also important to note that the method presented by Weitzenböck et al. [10] includes further detail on necessary adjustments for an inlet radius that is not consistent with the shape of the advancing flow front (since typically a simple circular inlet is employed, even for anisotropic materials). While this consideration is accounted for in this work, it requires some iteration from an initial estimate of the material anisotropy for each test. In any case, the 3 mm inlet is expected to have minimal impact on the greater flow front measurements [10], which range up to 120 mm.

Based on the principal permeability values, an effective permeability, K_{eff}, can also be calculated for any flow direction, θ, relative to the principal axes according to Eq. 9:

$$K_{eff} = \frac{K_1 K_2}{K_1 \sin^2\theta + K_2 \cos^2\theta} \qquad (9)$$

This effective permeability calculation relies on prior definition of the principal permeability values, however, the testing approach in this article allows for permeability calculations to be performed in a large number of directions (limited only by the digital image resolution). Hence, as the number of measurement directions becomes significant, the isotropic model in Eq. 5 can provide a detailed definition of permeability in all directions that is comparable to the effective permeability in Eq. 9, but also accounts for and displays any real variance. For many experimental approaches, particularly those using imbedded sensors, automatic measurement of the flow front in as few as three directions may lead to greater error. This problem is directly addressed in this research, both through raw, directional permeability calculations, and by repeating the three-direction approach for a statistically significant number of orientations in each test to ensure convergence of the K_1 and K_2 values. The importance of this point is discussed further with the experimental results, presented later in this article.

Code Implementation

To facilitate the calculation of anisotropic permeability (based on the above methods) from the experimental test video footage, an automated MATLAB code was developed. This code is freely available on the MathWorks file exchange website with supporting documentation [34]. It is designed to track the flow front of the fluid throughout test video footage, and ultimately performs permeability calculations using both the raw directional approach and the three-direction method (for any number of orientations). Similar efforts to develop an automated MATLAB code have been previously demonstrated [23]; however, this work required manual conversion and processing of

images in other software prior to analysis, while the presented core simply accepts video footage taken directly from the digital camera.

In order to determine the porosity, ϵ, (based on an approximation of fiber volume fraction, V_f) and the subsequent permeability of the fabric, several input parameters are required: the number of material plies, n, height of the test cavity, h, and fabric shear angle, γ, as well as material properties such as areal density, ρ_A, and fiber density, ρ_f. This relationship is shown in Eq. 10, though it is also important to note that as fabrics are sheared, the areal density, fiber volume fraction and porosity do not remain constant. Hence, the undeformed areal density, ρ_A^0, (0.193 kg/m^2) is divided by the cosine of the shear angle to find an improved approximation, as seen in Eq. 11.

$$\varepsilon = 1 - V_f, \; V_f = \frac{n\rho_A}{\rho_f h} \qquad (10)$$

$$\rho_A = \frac{\rho_A^0}{\cos\gamma} \qquad (11)$$

For each test the viscosity and differential pressure also need to be specified. Additionally, a scalar reference has to be assigned in order to convert distances from the video-native pixels to meters, along with the definition of the inlet radius. Depending on the clarity of the flow front progression, and the desired output of the code, there are also several modifiable video processing parameters.

The core of the MATLAB code relies on three loops, progressing through *time*, *angle*, and *radius* values respectively, as demonstrated in Fig. 3. The outer *time* loop operates on a pair of video frames with known time spacing between them, δt, iteratively proceeding through the sequence by updating video frames until the end of the test. These two frames are compared to effectively highlight changes between the frame at time t and the frame at time $t + \delta t$. For an ideal frame pair (without excessive noise or lighting changes) this results in a clear elliptical annular shape caused by the difference in the radial flow of fluid from the first frame to the second. The differential image from this process is then filtered using a pill-box (or disk) filter to reduce the effect of noise, and converted to a binary format, determined by a specified pixel intensity cut-off value. The optimal values for filter size and intensity cut-off, need to be determined by the operator to ensure the clarity of the elliptical annular shape in the image processing. For example, a typical filter of 5 pixels was used along with a 0.02 intensity cut-off. However, under similar experimental conditions these values should remain consistent across all tests once determined.

The nested *angle* loop simply sweeps through a range of flow directions (0 to 2π radians) while the last nested *radius* loop incrementally increases a radial length parameter, r, by δr from the inlet point until the annular flow front is detected. This distance corresponds to the flow
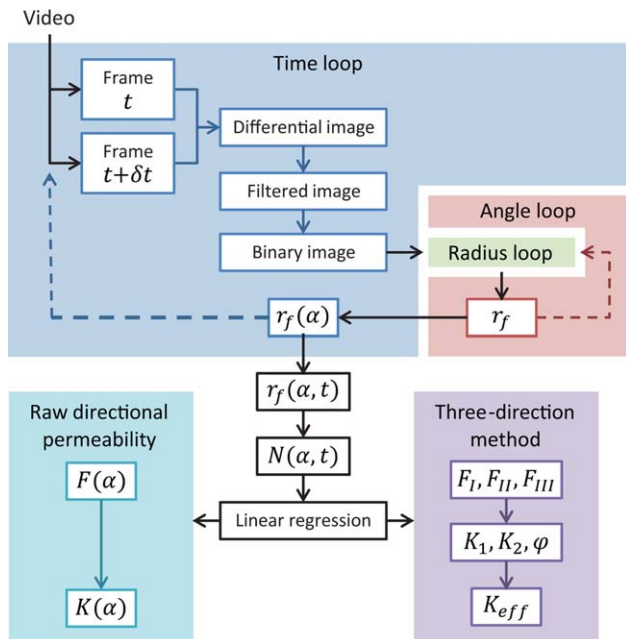
FIG. 3. Flowchart of the video processing code for tracking the radial flow front and calculating permeability based on two possible methods: raw directional permeability and the three-direction method [10]. [Color figure can be viewed at wileyonlinelibrary.com]

front radius, r_f, of the first image in the frame pair at time t, for the current angle. Once the entire flow front is defined for the current time as a function of direction, $r_f(\alpha)$, the frame pair is incremented forward in time and the whole process is repeated. Ultimately, by the end of the *time* loop, the complete flow front history is known as a function of both time and direction, $r_f(\alpha, t)$.

From the discrete values of flow front radius (for every time increment and direction), the bracketed flow front term from *Eq. 5* is calculated (termed N for convenience) according to *Eq. 12*.

$$N = \left[r_f^2 \left(2\ln \left(\frac{r_f}{r_0} \right) - 1 \right) + r_0^2 \right] \quad (12)$$

Thus, this can be expressed as a discrete function of t and α, which is represented as $N(\alpha, t)$ in Fig. 3. The MAT-LAB code includes two different permeability characterization methods (as described in the previous section), which both rely on a linear time regression of $N(\alpha, t)$. The first is a calculation of raw directional permeability, $K(\alpha)$, based on *Eq. 5* for each of the measured directions (the number of which is chosen by the operator). Alternatively, the three-direction method by Weitzenböck et al. [10] is employed according to *Eq. (6–8)* for every possible triplet of measured directions (0°, 45°, and 90° relatively). This approach provides estimates of principal permeability values, K_1 and K_2, and principal direction, φ, from each triplet for statistical analysis. From these properties it is also possible to calculate an effective permeability, K_{eff}, in every direction according to *Eq. 9* that

is an approximation comparable to the raw directional permeability results.

EXPERIMENTAL RESULTS

Observations and Regression Analysis

Video footage was recorded in high definition (1,920 × 1,080 pixel resolution) for subsequent processing in the MATLAB code [34], resulting in approximately 23 pixels per millimeter across the test samples. Moderate changes in lighting conditions during testing had minimal effect on the video processing. Overall, the flow behavior during the tests was observed to be consistent with expectations, where, for example, the unsheared plain weave fabric facilitated a near circular and isotropic flow front as shown in Fig. 4. In agreement with theory, fluid flow for each test was initially quite rapid and decelerated as the flow front advanced under the constant pressure control. For tests with the lowest oil viscosity, μ, (0.08046 Pa s) and an oil surface tension, σ, of 0.032 N/m, fluid velocity, u, was observed to range from 0.0004 m/s at the end of testing to above 0.0022 m/s near the inlet. Subsequently the capillary number, Ca, can be calculated according to *Eq. 13*, resulting in a range of 1.0E-3 to 5.5E-3 for viscous dominated flow.

$$Ca = \frac{\mu u}{\sigma} \quad (13)$$

In the tests with sheared material, the elliptical flow front was a clear indication of anisotropy, which is shown for several samples in Fig. 4 (75 s into each experiment). Deviations from a perfectly elliptical shape can be observed in the highlighted flow fronts, reflective of the variance that is common in radial permeability experiments.

Regression analysis was performed to ensure that the flow assumptions under constant pressure were reasonable for the construction of the term N in *Eq. 12*. In theory, a non-linear trend in the calculated N values over time might suggest that capillary driven flow was significant. However, the results consistently displayed a very high degree of linearity (with R^2 values typically greater than 0.99 for each regression fit). This linearity also supports the assertion that any spatial variations in cavity thickness were negligible and that any influence of plate deformation was minimal. Figure 5 shows regression fits of the N terms against time for the principal permeability direction, φ, and two additional 45° increments in the measurement orientation, from a 20° shear-angle sample. These regression results are representative of the trends from every direction of each test.

Raw Directional Permeability

First, to qualitatively compare similar tests, the raw directional permeability results are shown for each test
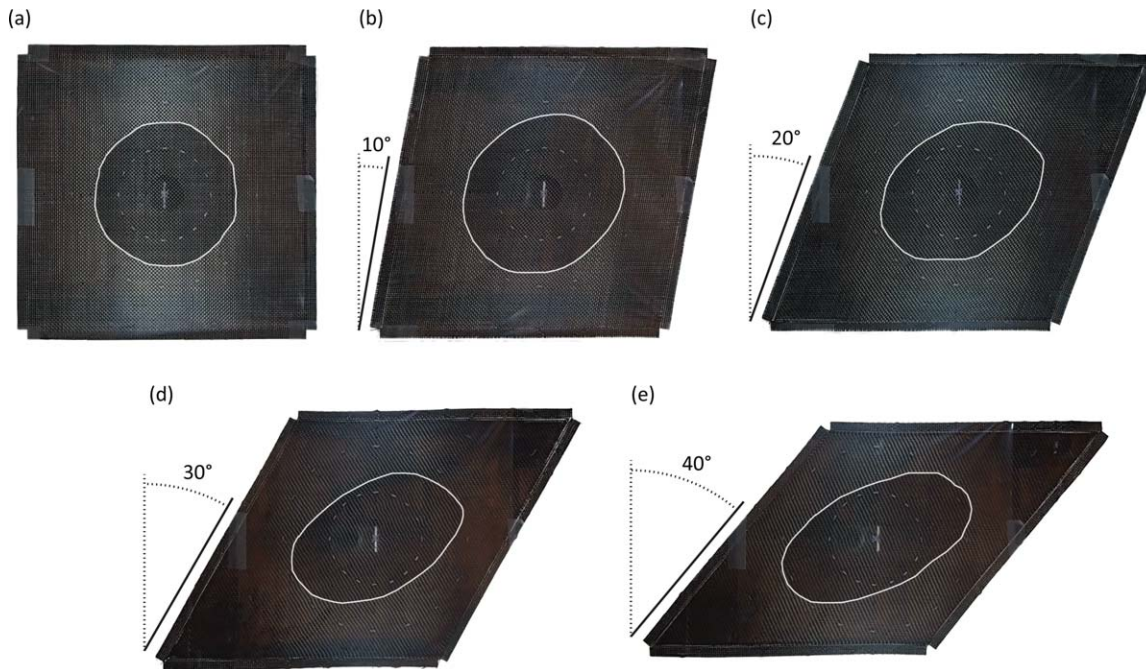
FIG. 4. Images from flow experiments (at 75 s) for, (a) 0° shear angle, (b) 10°, (c) 20°, (d) 30°, and (e) 40°. Flow front profiles are highlighted for clarity. [Color figure can be viewed at wileyonlinelibrary.com]

batch in Fig. 6. These results are all displayed relative to the test conditions (Fig. 4) where warp yarns were aligned with the horizontal direction, and weft yarns were sheared to the desired angles (as depicted by the solid black lines in Fig. 6). Each dimensionally-similar radial plot consists of the five to six directional permeability curves from a particular shear angle batch and a black dashed curve that depicts the average.

The symmetric permeability curves presented in Fig. 6 are a result of the near-elliptical flow front behavior observed during testing (since permeability depends on the square of flow front radius). Tests conducted at 0°, 10°, and 20° shear show greater variance between repeated tests, with relative standard deviations for each direction ranging from ±20% to 30%. At 30° and 40° though, this reduces to ±4% to 15%, showing a significant improvement in repeatability that is reflected qualitatively in Fig. 6 by the similarity of tests. This improved repeatability may be the result of tighter spacing that reduces the freedom for local deformation and stochastic/systematic variability. The experimental scheme, which rotated the testing order of samples from different batches, ensured that this observation was not simply due to any technical improvement. Unsheared (0°) samples generally exhibit the expected isotropic permeability behavior, despite flow irregularities occurring in some tests. Overall, as the shear angle increases, the anisotropy of the permeability is also seen to increase. Furthermore, the results for each sheared batch of samples appear to show peak permeability values in the bias direction, directly between the two yarn directions, likely as a result of tow gap alignment facilitating the most flow.

Three-Direction Method

For each individual test, a total of 64 measurement directions were recorded using the video processing code (at 5.625° increments). Defining each measurement direction as the first of a 0°, 45°, and 90° triplet (*I*, *II*, and *III* according to Fig. 2), the three-direction method [10] has been employed to find 64 different approximations of K_1, K_2, and φ for each test based on each of the possible triplet orientations.

Figure 7 depicts the distribution of principal permeability results for every possible orientation using the three-direction method, where markers represent the average for each test and error bars represent the standard deviation. Dashed lines of anisotropy (the ratio of K_1/K_2) are drawn as linear trend lines. As noted from the raw permeability results, the unsheared (0°) samples are nearly
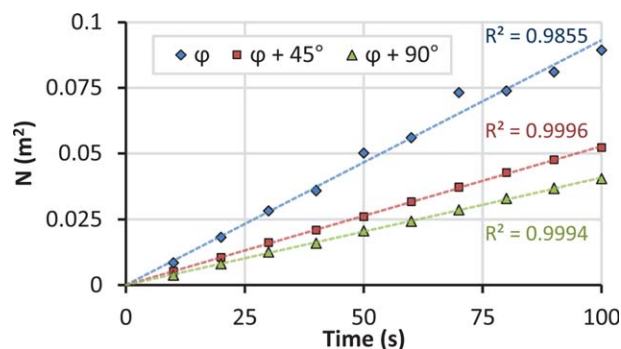

FIG. 5. Linear time regression of *N* terms from a 20° shear angle specimen, for the principal permeability direction, φ, and increments of 45° and 90°. [Color figure can be viewed at wileyonlinelibrary.com]
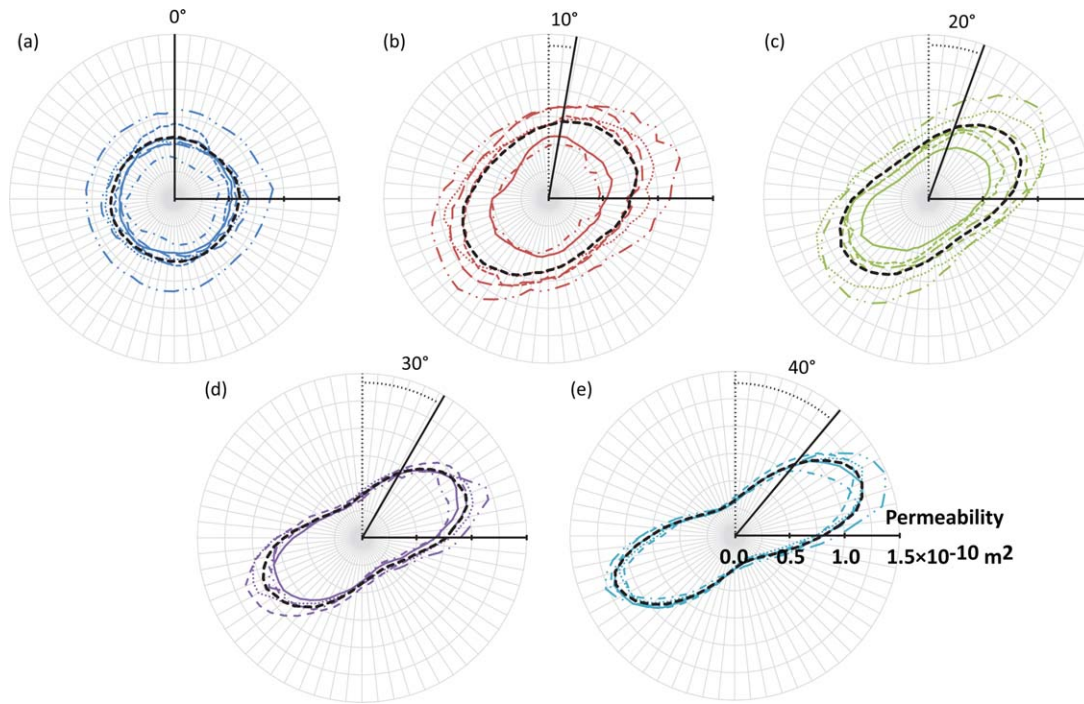
FIG. 6. Raw directional permeability results for, (a) 0° shear angle, (b) 10°, (c) 20°, (d) 30°, and (e) 40°. Average curves are represented as black dashed lines for each batch. [Color figure can be viewed at wileyon-linelibrary.com]

isotropic, with a principal permeability ratio of 1.13. The anisotropy then steadily increases with the shear angle, up to a ratio of 3.71 for the 40° test batch.

Comparing results from like tests, the prediction of anisotropy is very consistent and accurate, with a relative standard deviation of ±6% for the unsheared case and less than ±4% for the sheared cases. This is unexpected

given the relatively large variation in the mean calculated K_1 and K_2 permeability values from test to test, particularly at lower shear angles (0°, 10°, and 20°) where the relative standard deviations are greater than ±20%. However, the mean principal permeability values between tests at 30° and 40° were actually quite consistent, with relative standard deviations of around ±7% and ±4%, respectively, again this is expected to be the result of tighter spacing between yarns.

The three-direction method not only calculates an estimate of principal permeability values, but also the direction to which they are oriented. Figure 8 relates the
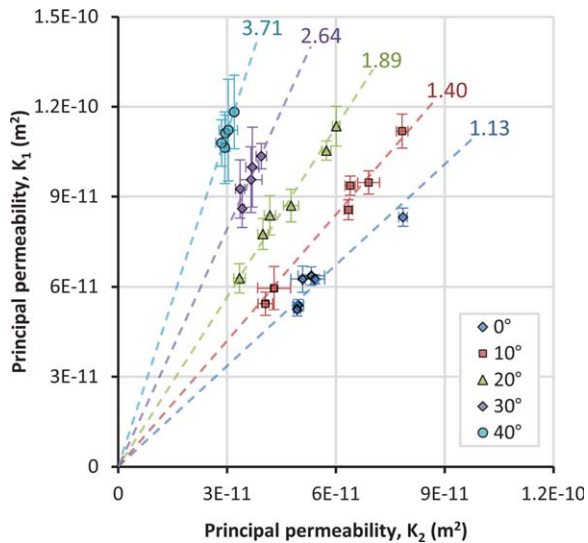

FIG. 7. Distribution of all the test results using the three-direction method at each shear angle with trend lines illustrating flow anisotropy. Each marker represents the mean principal permeability estimates from a single test, with error bars showing the standard deviation. [Color figure can be viewed at wileyonlinelibrary.com]
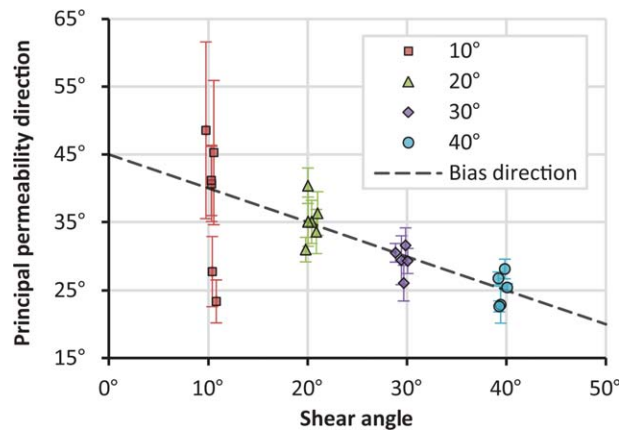

FIG. 8. Distribution of the predicted principal permeability directions for each test using the three-direction method, as compared with the fabric bias direction for increasing shear angles. [Color figure can be viewed at wileyonlinelibrary.com]
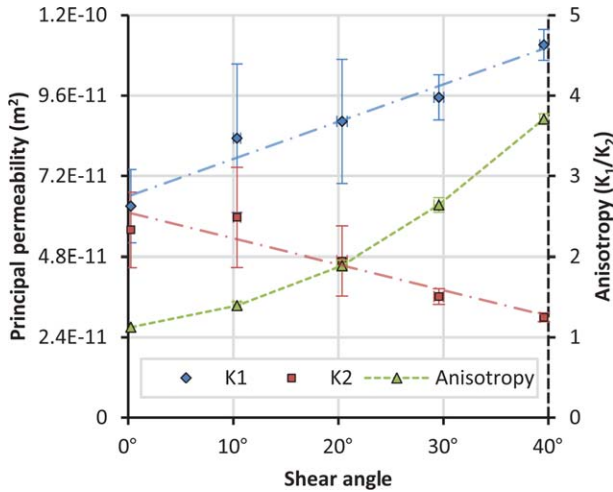
FIG. 9. The relationship between principal permeability values, anisotropy, and the fabric shear angle. Linear trend lines have been added for the principal permeability data. [Color figure can be viewed at wileyonlinelibrary.com]

samples of different shear angles with the estimated principal permeability directions using the three-direction method results for all orientations. The standard deviation of the calculated principal permeability directions are plotted as vertical error bars. Results from unsheared samples are not shown as the flow is near isotropic and, as such, the principal permeability directions are not clear, nor necessary. Similarly, the 10° shear samples show very high variability as the anisotropy is still relatively low. At higher shear angles the tests appear to be more repeatable

and reliable in terms of determining the principal permeability direction, with relative standard deviations ranging from ±2% to 12%. The line of the bias direction (bisecting the two yarn directions) is also shown on the figure, which correlates very well with the mean results from each batch. This shows that for this particular plain weave fabric the bias direction can be assumed to be the K_1 principal permeability direction.

Figure 9 displays more clearly the mean principal permeability and anisotropy trends from Fig. 7, in relation to the increasing shear angle. As noted earlier, the error in K_1 and K_2 values is relatively large at lower shear angles, improving for the 30° and 40° samples, though it is the minimal error in the anisotropy of samples at all shear angles that is most interesting. The general trends are also evident: as shear angle increases, K_1 values increase and K_2 values decrease, and consequently the anisotropy increases greatly.

The averaged raw experimental results for permeability in every direction (from Fig. 6) are compared in Fig. 10 against the mean effective permeability, K_{eff}, of all the statistical three-direction approximations. Overall, the general shape and magnitude are well captured by both approaches.

Error Evaluation

The video processing approach used in this article allows for any number of measurement directions to be employed. In this work, 64 measurement directions have
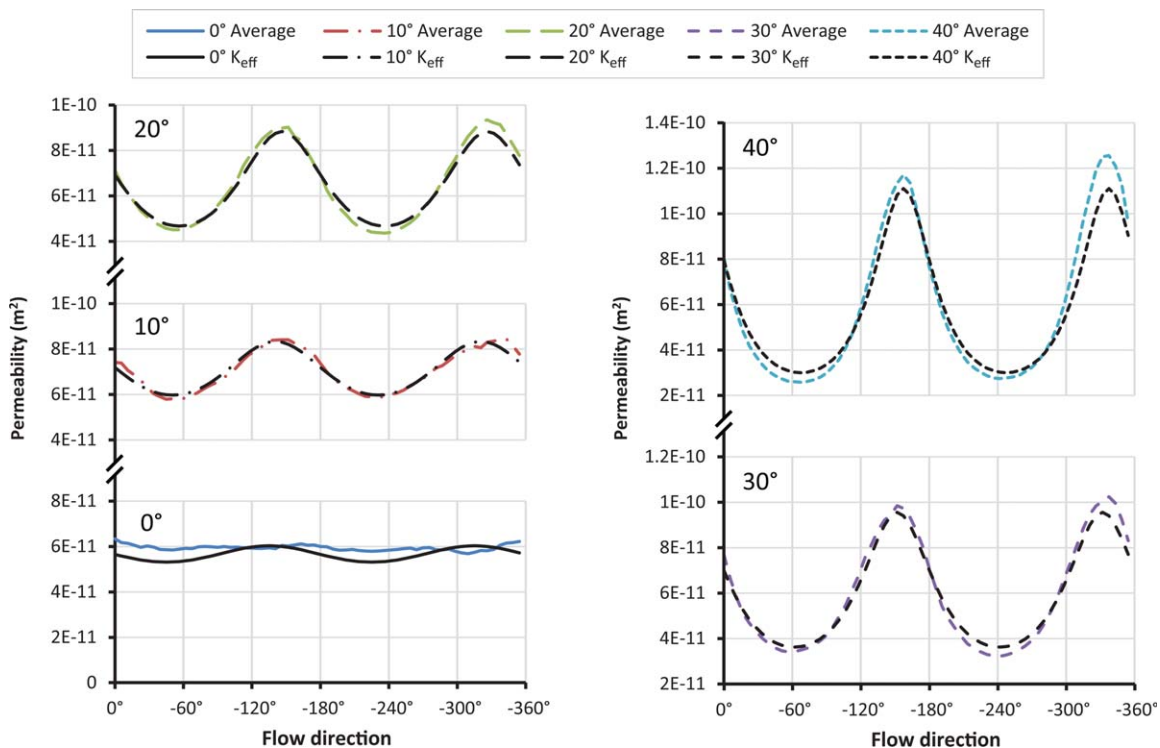

FIG. 10. Comparison of average raw directional permeability (from Fig. 6) and calculated effective permeability for each of the shear angle batches. [Color figure can be viewed at wileyonlinelibrary.com]
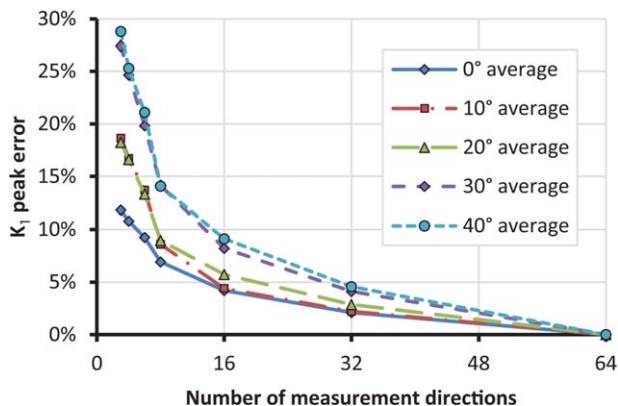
FIG. 11. Average peak error for each shear angle batch based on the number of measurement directions used to calculate a K_1 estimate, relative to results from 64 measurement directions. [Color figure can be viewed at wileyonlinelibrary.com]

been studied for a reliable characterization of the mean permeability results. However, many experimental methods rely on far fewer measurement directions, assuming that the experimental flow front will be close to a perfect ellipse and that error will therefore be small.

For instance, some early experimental procedures relied on sensor measurements from only three directions (the minimum required for characterizing permeability using the three-direction method) [10, 35]. The advantage of such sensor rigs is that they can tightly control cavity thickness and compaction, however, they are more difficult and expensive to set up than the approach outlined in this article. Other sensor implementations increased the number of measurement directions to 7 [36] or 16 [37], although this is still a relatively low number compared with the 64 measurement directions used in this research.

In order to evaluate this source of potential error, K_1 and K_2 estimates were calculated for all possible subset combinations of 3, 4, 6, 8, 16, and 32 measurement directions in each test to compare against the K_1 and K_2 values determined for all 64 measurement directions. Hence, the mean and peak relative error was found for each of the principal permeability estimates in relation to the number of measurement directions. Overall, the relative errors of the K_2 estimates were quite low, with average peak error below 10% and mean error below 4% for the case of only three measurement directions (the minimum required to perform the calculations). However, the relative error of the K_1 estimates showed much greater variability. For the unsheared batch of samples, K_1 error was similar to K_2 error (since the flow is near-isotropic), but as the shear angle increased the average peak K_1 error increased to 28.8%. As expected, an increasing number of measurement directions reduces the relative error in all cases, such that even the 40° shear sample batch only observes an average peak K_1 error of 9.1% when 16 measurement directions are used. Figure 11 shows the average peak K_1 error for each shear angle batch in relation to the number of measurement directions, in particular, highlighting the

convergence of relative error as the number of measurement directions increases.

Ultimately for these experiments, the natural flow front variability suggests that reliable permeability characterization should be based on at least 16 measurement directions to ensure that mean error is below 5% and any potential peak error is below 10%.

DISCUSSION

The main advantage of the method employed in this article, is the complete directional definition of permeability for each test from a simple and low-cost experiment. Since optical radial tests can provide data in all directions simultaneously, they can be used to improve the statistical reliability and remove the possibility of operator bias in the prediction of principal permeability values. The analysis in section "Error Evaluation" shows that using the three-direction permeability characterization method with data from fewer than 16 measurement directions for these tests could result in significant error. This is particularly true for the tests at higher shear angles, where it has been shown that the variance in K_1 resulting from consideration of only three measurement directions is greater than the batch experimental variance. The statistical mean results show very good consistency in terms of anisotropy between like tests, and also show good agreement with the raw experimental permeability distributions (as seen in Fig. 10). This is also a very low cost experimental method, without the need for sophisticated sensors or complicated sensor arrangements, whilst still allowing measurement and analysis to be largely automated. Moreover, the extensive data available from this approach enables a detailed statistical analysis of each permeability test, and allows for better interpretation of the results. This flow front tracking and analysis code has also been made freely available on the MathWorks file exchange website [34]. Recently, other researchers have demonstrated similar automated tools for visual flow front tracking and local shear angles in deformed samples [38]. Their work also observed increasing anisotropy with shear angle, along with a rotation of the principal permeability direction (relative to the twill-weave fiber directions) that is similar to the results reported in this article.

Often, experimental permeability testing is performed on thicker, multiple-ply samples, rather than a single fabric layer (as in this case) to reduce the influence of wall effects and better represent a typical layup with a fiber volume fraction closer to 0.5. However, it is also well documented that variations in the way layers are stacked results in different degrees of "nesting," and can significantly alter the permeability [39], in some cases by as much as an order of magnitude [20]. Hence, a single-ply test was chosen at this stage of the research to eliminate this effect, particularly in support of infusion modeling for single-ply experiments [8]. However, the use of a single layer and constant cavity thickness meant that, with

this particular plain weave material, the fiber volume fraction (which ranged from 0.28 to 0.36) was lower than is typical for an aerospace grade part, though it is not unprecedented in similar research [31]. Despite this, the reduced fiber volume fraction and wall effects on fluid flow were deemed acceptable, since the purpose of this research was to demonstrate both the method and the relative relationship between shear angle and permeability as consistently as possible.

Naturally, in order to extend this method to practical applications for industry, a broader range of permeability tests for thicker layups would be necessary to capture the behavior at higher fiber volume fractions and with different alignments of the layers.

CONCLUSION

Radial permeability testing was performed over a range of shear angles for a plain weave, carbon-fiber, textile reinforcement. Experiments were run under a constant vacuum with flow front progression being monitored with a digital video camera. A new MATLAB code was developed to process the video footage, track the flow front and subsequently calculate the permeability in all directions.

From this comprehensive data, a statistical mean set of K_1 and K_2 values was determined for greater confidence. This process revealed the refined anisotropy of samples at each shear angle to be very consistent, despite some variance in principal permeability values.

Overall, test samples with a greater degree of shearing showed greater anisotropy, higher K_1 values and lower K_2 values. The effective mean principal permeability values showed good agreement with the results determined from the raw directional permeability calculations. However, using the traditional methods with fewer than 16 measurement directions could result in significant error due to irregularities that are common in permeability experiments particularly at high shear angles. It is only by taking the data from all directions that the method employed in this article has been able to reduce the error in measuring principal permeabilities with greater confidence. The results from this work also serve as a significant contribution to the development of multidisciplinary process models for the LCM of structures with considerable curvature and complexity, where localized permeability and flow behavior can change as a result of fabric deformation [8].

ACKNOWLEDGMENTS

References

1. P. Badel, S. Gauthier, E. Vidal-Sallé, and P. Boisse, Compos. Part a Appl. Sci. Manuf., **40**, 8 (2009).

2. P. Boisse, M. Borr, K. Buet, and A. Cherouat, Compos. Part B Eng., **28**, 4 (1997).

3. X.Q. Peng, and J. Cao, Compos. Part a Appl. Sci. Manuf., **36**, 6 (2005).

4. D. Durville, Int. J. Mater. Form., **3**, 1241 (2010).

5. M.K. Kang, W.I. Lee, and H.T. Hahn, Compos. Part a Appl. Sci. Manuf., **32**, 11 (2001).

6. E.M. Sozer, S. Bickerton, and S.G. Advani, Compos. Part a Appl. Sci. Manuf., **31**, 12 (2000).

7. G. Tuncol, A.C. Loos, and R.J. Cano, 18th Int. Conf. Compos. Mater., Jeju Island, Korea (2011).

8. R.S. Pierce, B.J. Falzon, and M.C. Thompson, 20th Int. Conf. Compos. Mater., Copenhagen, (2015).

9. K.L. Adams, W.B. Russel, and L. Rebenfeld, Int. J. Multiph. Flow, **14**, (1988).

10. J.R. Weitzenböck, R.A. Shenoi, and P.A. Wilson, Compos. Part a Appl. Sci. Manuf., **30**, 6 (1999).

11. J.R. Weitzenbock, R.A. Shenoi, and P.A. Wilson, Compos. Part a Appl. Sci. Manuf., **29**, 159 (1998).

12. C.H. Park, A. Lebel, A. Saouab, J. Bréard, and W. Lee, Compos. Part a Appl. Sci. Manuf., **42**, 658 (2011).

13. R. Arbter, J.M. Beraud, C. Binetruy, L. Bizet, J. Bréard, S. Comas-Cardona, C. Demaria, A. Endruweit, P. Ermanni, F. Gommer, S. Hasanovic, P. Henrat, F. Klunker, B. Laine, S. Lavanchy, S.V. Lomov, A. Long, V. Michaud, G. Morren, E. Ruiz, H. Sol, F. Trochu, B. Verleye, M. Wietgrefe, W. Wu, G. Ziegmann. Compos. Part a Appl. Sci. Manuf., **42**, 1157 (2011).

14. F. Gommer, L.P. Brown, and R. Brooks, J. Compos. Mater., **77**, 266 (2015).

15. N. Vernet, E. Ruiz, S. Advani, J.B. Alms, M. Aubert, M. Barburski, et al. Compos. Part a Appl. Sci. Manuf., **61**, (2014).

16. C.C. Wong, A.C. Long, M. Sherburn, F. Robitaille, P. Harrison, and C.D. Rudd, Compos. Part a Appl. Sci. Manuf., **37**, 6 (2006).

17. F. Loix, P. Badel, L. Orgéas, C. Geindreau, and P. Boisse, Compos. Sci. Technol., **68**, 7 (2008).

18. B. Verleye, S.V. Lomov, A. Long, I. Verpoest, and D. Roose, Compos. Part a Appl. Sci. Manuf., **41**, 1 (2010).

19. A. Hammami, F. Trochu, R. Gauvin, and S. Wirth, J. Reinf. Plast. Compos., **15**, 1108 (1996).

20. F.D. Dungan, M.T. Senoguz, A.M. Sastry, and D.A. Faillaci, J. Compos. Mater., **35**, 14 (2001).

21. N. Takano, M. Zako, T. Okazaki, and K. Terada, Compos. Sci. Technol., **62**, 10 (2002).

22. K. Okonkwo, P. Simacek, S.G. Advani, and R.S. Parnas, Compos. Part a Appl. Sci. Manuf., **42**, 10 (2011).

23. R. Loendersloot. Thesis. University of Twente (2006).

24. S. Sharma and D.A. Siginer, Appl. Mech. Rev., **63**, 2 (2010).

25. T.S. Lundström, R. Stenberg, R. Bergström, H. Partanen, and P.A. Birkeland, Compos. Part a Appl. Sci. Manuf., **31**, 1 (2000).

26. A. Endruweit, P. McGregor, A.C. Long, and M.S. Johnson, *Compos. Sci. Technol.*, **66**, 11 (2006).

27. S.H. Ahn, W.I. Lee, and G.S. Springer, *J. Compos. Mater.*, **29**, 6 (1995).

28. Y. Luo, I. Verpoest, K. Hoes, M. Vanheule, H. Sol, and A. Cardon, *Compos. Part a Appl. Sci. Manuf.*, **32**, 10 (2001).

29. A. Endruweit and P. Ermanni, *Compos. Part a Appl. Sci. Manuf.*, **35**, 4 (2004).

30. J. Slade, E.M. Sozer, and S.G. Advani, *J. Reinf. Plast. Compos.*, **19**, 7 (2000).

31. P. Smith, C.D. Rudd, and A.C. Long, *Compos. Sci. Technol.*, **57**, 3 (1997).

32. C.-L. Lai and W.-B. Young, *Polym. Compos.*, **18**, 5 (1997).

33. L.M. Diamante and T. Lan, *J. Food Process.*, **2014**, (2014).

34. R.S. Pierce, *Video processing for permeability characterisation - File exchange - MATLAB Central*, http://www.mathworks.com/matlabcentral/fileexchange/48002-video-processing-for-permeability-characterisation.

35. K.K. Han, C.W. Lee, and B.P. Rice, *Compos. Sci. Technol.*, **60**, 12 (2000).

36. K. Hoes, D. Dinescu, H. Sol, R.S. Parnas, and S. Lomov, *Compos. Part a Appl. Sci. Manuf.*, **35**, 12 (2004).

37. Q. Liu, R.S. Parnas, and H.S. Giffard, *Compos. Part a Appl. Sci. Manuf.*, **38**, 3 (2007).

38. P.-J. Liotier, Q. Govignon, E. Swery, S. Drapier, and S. Bickerton, *J. Compos. Mater.*, **49**, 27 (2015).

39. S.V. Lomov, I. Verpoest, T. Peeters, D. Roose, and M. Zako, *Compos. Sci. Technol.*, **63**, 7 (2003).